A 6.78 MHz Wireless Power Transfer System for Simultaneous Charging of Multiple Receivers with Maximum Efficiency using Adaptive Magnetic Field Distributor IC

Hao Qiu[1,2], Makoto Takamiya[1]
[1]The University of Tokyo, Tokyo, Japan; [2]Now with Nanjing University, Nanjing, China. Email: qiuhaonju@gmail.com

Abstract

We developed a 6.78 MHz wireless power transfer (WPT) system for simultaneous charging of multiple receiver (RX) coils. On the basis of the transmitter (TX)-RX and RX-RX coupling distinguished by the adaptive magnetic field distributor (AMFD) IC, the distribution of magnetic fields from the TX coils was optimized at each RX coil for the maximum efficiency. A 2-TX 2-RX WPT system was implemented with the AMFD ICs fabricated in 1.8 V, 180 nm CMOS process. Compared with the conventional method, the system efficiency is increased from 8.9 % to 61 % with the load power of 173 mW.

Introduction

With an explosive increase of users, as shown in Fig. 1, a WPT system that supports simultaneous wireless charging of multiple RXs with maximum efficiency is highly desirable. The conventional method like turning on a single TX coil, as shown in Fig. 2(a), cannot effectively transfer power wirelessly to the RX coils when the coupling between TX coil 2 and the RX coils is weak. Using multiple TX coils without control, as shown in Fig. 2(b), is not a good method either since the magnetic fields generated by the TX coils can cancel out at the RX coils. The worst case is no power can be transferred to the RX coils.

On the other hand, as shown in Fig. 2(c), by controlling the current in each TX coil on the basis of the TX-RX and RX-RX coupling, the distribution of magnetic fields from the TX coils can be optimized at different RX coils to achieve the maximum efficiency. Several previous works on a multiple TX WPT system have been reported [1-3]. However, all these works only support wireless charging of a single RX coil. When the number of the RX coils is greater than 1, taking [3] as an example, since they are coupled with the TX coils at any point in time, the integrated k sensor cannot distinguish between them. Moreover, the RX-RX coupling cannot be known either. As a result, the optimized current in each TX coil cannot be correctly computed for the optimized distribution of magnetic fields at different RX coils.

In this work, by distinguishing between the coupling coefficients (ks) between each pair of coils (TX-RX and RX-RX) using the AMFD IC, we developed a WPT system for simultaneous charging of 2 RX coils with the maximum efficiency.

Adaptive Magnetic Field Distributor IC

Fig. 3 shows a block diagram of the WPT system, consisting of 2 TX coils driven by 2 AMFD ICs (TX1 and TX2), 2 RX coils, and a top controller. According to the theoretical analysis in [4], the TX-RX and RX-RX coupling can be calculated by tentatively turning on TX coils and measuring the current and voltage of each TX coil. To achieve this without using current and voltage probes which are bulky and costly, a current and voltage sensor is integrated in each AMFD IC, which also consists of two half-bridges (HBs) and related digital control. AMFD ICs TX1 and TX2 firstly measure the currents and voltages in TX coils 1 (I_1, V_1) and 2 (I_2, V_2) and output the results to the top controller for the calculation of the TX-RX and RX-RX coupling. After that, the AMFD ICs drive HBs [3] to adjust the current in each TX coil to its optimal value for the maximum system efficiency.

For the coil current sensing, we obtain it by differentiating the voltage across the capacitor in the coil, considering that the sensing resistor may introduce power loss and the transformer cannot be integrated. However, the current sensing accuracy can be degraded due to the process variation of the RC time constant in the operational amplifier (op-amp) differentiator. To solve this problem, a calibration technique is proposed, as shown in Fig. 4(a).

During the calibration, the RX coils are absent. Take TX coil 1 as an example. Since it is resonated at the resonance frequency (f_0), the amplitude of voltage across the inductor L_1 (V_L) equals that across the capacitor C_1 (V_C). These high-level voltages are attenuated and result in V_{L1} and V_{C1}. V_{L2} is obtained by integrating V_{L1} and V_{C2} is obtained by differentiating V_{C1} over time. As V_{L2} and V_{C2} are AC voltages, their peak values are stored as V_{L3} and V_{C3} by the sample-and-hold (S&H) circuits at proper instants. The corresponding equations are listed in Fig. 4(b). The calibration is executed and will end up with V_{L3} equal to V_{C3}, as shown in Fig. 4(c). According to the comparison results, the 5-bit R is controlled by the logic circuits to calibrate the RC time constants of both op-amp integrator and differentiator. After calibration, R remains unchanged and the RC time constant equals $1/(2\pi f_0)$, and the coil current (I_1) can be accurately obtained with the peak value as AMP_I, since L_1, C_1, and the attenuation ratio (β) have been known. The calibration procedure guarantees a correct current measurement for the calculation of the TX-RX and RX-RX coupling and the optimized current in the top controller.

The coil voltage (V_1) passes the attenuator, and its peak value is obtained as AMP_V by the S&H circuit. The phase between V_1 and I_1 is obtained as PHASE by two zero-crossing detectors followed by an XOR gate and a low pass filter (LPF).

Experimental Results

Fig. 5 shows a die photograph of AMFD IC fabricated in 1.8 V, 180 nm CMOS. The die size is 1.90 mm x 1.83 mm. All TX and RX coils are 10-turn flexible PCB coils with the outer diameter of 50 mm. The load resistances (R_{LS}) are 10 Ω. f_0 is 6.78 MHz. Fig. 6 shows the measured waveforms during the calibration of the coil current sensor. β is 0.01. EN is the calibration enabled signal and is generated off-chip. STATE indicates the state of calibration and goes to LOW when the calibration ends. The system enters normal operation after calibration.

Figs. 7(a), 8(a), and 9(a) show the measurement setups, in which the RX coils are perpendicular to the TX coils. 3 cases are listed, in which RX coil 1 is perpendicular to (case 1) or parallel with (cases 2 and 3) RX coil 2. On the basis of the measurement results of the AMFD ICs, the top controller calculates the ks as shown in Figs. 7(b), 8(b), and 9(b) and the optimized current for each TX coil. The optimized currents in TX coils 1 and 2 are measured and shown in Figs. 7(c), 8(c), and 9(c). The measured load power is shown in Figs. 7(d), 8(d), and 9(d), and the measured system efficiency (η_{SYS}) is shown in Figs. 7(e), 8(e), and 9(e).

Compared with all three conventional methods (TX coil 1 on, TX coil 2 on, and TX coils 1 and 2 on without control), our proposed method shows great performance improvement. In case 1, η_{SYS} is increased from 8.9 % to 61 % with the load power of 173 mW. Similarly, η_{SYS} is increased from 3.9 % to 19 % with the load power of 68 mW in case 2 and increased from 2.6 % to 47 % with the load power of 183 mW in case 3. Relatively high performance can be obtained by selectively turning on TX coil 1 or 2. However, this requires that the status of R_{LS} be transmitted to the TX side and will make the system complex. On the other hand, no TX-RX communication link is required in this work. Table I shows a comparison table summarizing related works on multiple TX WPT systems. This work achieves simultaneous charging of multiple RX coils with maximum efficiency.

Acknowledgement

This work was partially supported by JST ERATO Grant Number JPMJER1501, Japan.

References

[1] B. H. Water *et al.*, *IEEE Trans. Power Elec.*, pp. 6298-6309, 2015. [2] D.-H. Kim *et al.*, *IEEE Trans. Power Elec.*, pp. 11391-11400, 2020. [3] H. Qiu *et al.*, *VLSI Circ.*, 2020, pp. 1-2. [4] G. Yang *et al.*, *IEEE Trans. Signal Process.*, pp. 2860-2874, 2017.

Fig. 1. Wireless charging of multiple RXs.

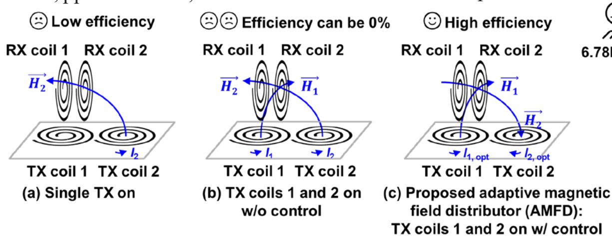

Fig. 2. (a)-(b) Conventional and (c) proposed WPT method.

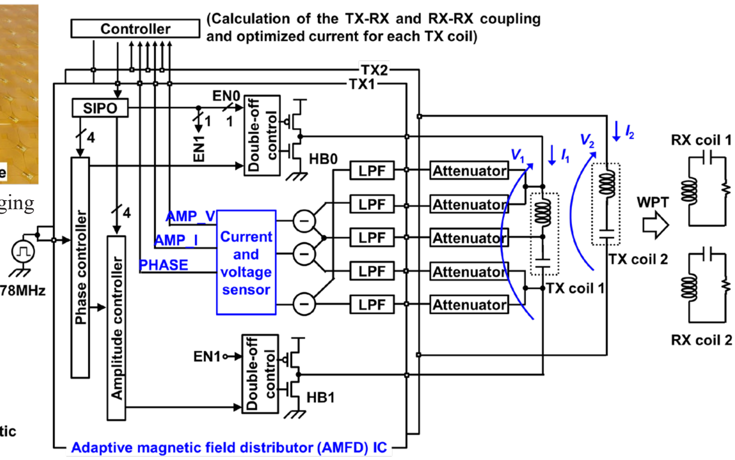

Fig. 3. Block diagram of the proposed WPT system.

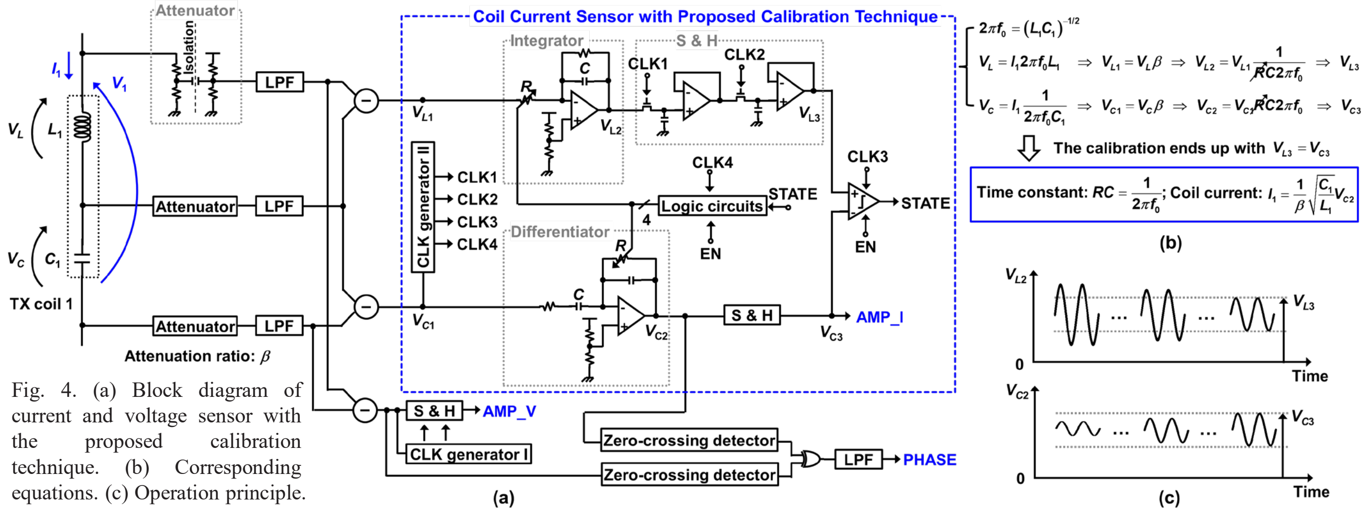

Fig. 4. (a) Block diagram of current and voltage sensor with the proposed calibration technique. (b) Corresponding equations. (c) Operation principle.

Fig. 7 (Case 1)

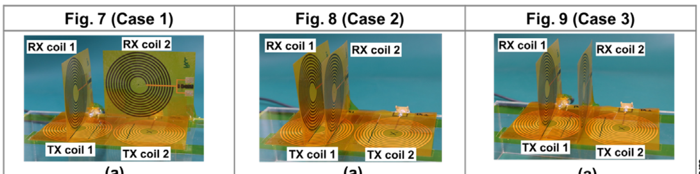

(a)

k	RX coil 1	RX coil 2
TX coil 1	~ 0	1.18 × 10^-2
TX coil 2	1.78 × 10^-2	5.23 × 10^-2
RX coil 1		2.43 × 10^-2

(b)

Optimized current	TX coil 1	TX coil 2
|I| (mA)	50	247
∠I (°)	0	0

(c)

Fig. 8 (Case 2)

(a)

k	RX coil 1	RX coil 2
TX coil 1	~ 0	1.02 × 10^-1
TX coil 2	1.85 × 10^-2	3.70 × 10^-2
RX coil 1		3.45 × 10^-2

(b)

Optimized current	TX coil 1	TX coil 2
|I| (mA)	340	150
∠I (°)	0	177

(c)

Fig. 9 (Case 3)

(a)

k	RX coil 1	RX coil 2
TX coil 1	~ 0	8.88 × 10^-2
TX coil 2	1.80 × 10^-2	8.92 × 10^-2
RX coil 1		1.31 × 10^-1

(b)

Optimized current	TX coil 1	TX coil 2
|I| (mA)	210	190
∠I (°)	0	200

(c)

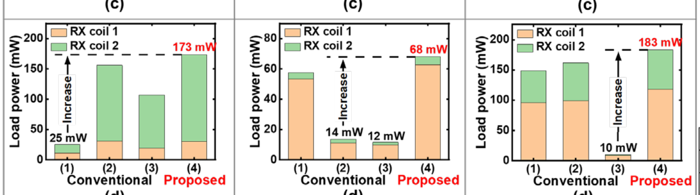

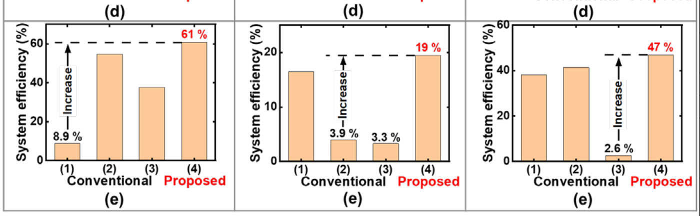

(a) Setup. (b) Calculated *k*. Measured (c) optimized coil current, (d) load power, and (e) system efficiency. Conventional (1) TX coil 1 on, (2) TX coil 2 on, (3) Both TX coils on w/o control. Proposed: Both TX coils on w/ control.

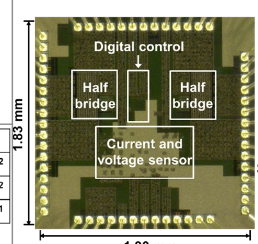

Fig. 5. Die micrograph.

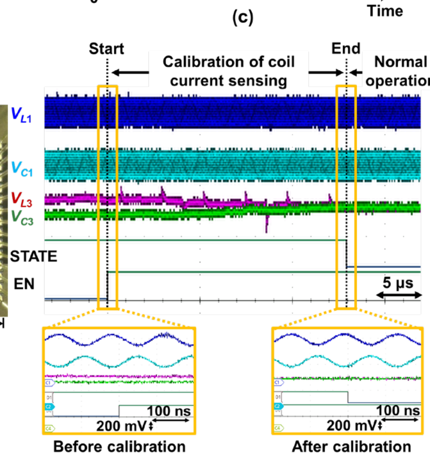

Fig. 6. Measured waveforms during calibration.

Table I. Comparison with Prior Art.

		[1]	[2]	[3]	This work
Implementation		Discrete	Discrete	180 nm CMOS	180 nm CMOS
Number of coils	TX	2 x 1	3 x 1	2 x 2	2 x 1
	RX	1	1	1	2
Charging of multiple RXs with maximum efficiency		No	No	No	Yes
Frequency		13.56 MHz	100 kHz	6.78 MHz	6.78 MHz
Supply voltage		10 V	N/A	1.8 V	1.8 V
Current sensing in each TX coil		N/A	N/A	N/A	Integrated current sensor with calibration technique
TX ⊥ RX	Load power	N/A	N/A	458 mW	183 mW
	WPT efficiency	N/A	N/A	48 %	61 %
	Distance*/TX size	N/A	N/A	1/2	1/2

* Distance between the center of the RX coil and TX coils.